The classical mutual information in mean-field spin glass models

Vincenzo Alba,[1] Stephen Inglis,[2] and Lode Pollet[2]

[1]*International School for Advanced Studies (SISSA), Via Bonomea 265, 34136, Trieste, Italy, INFN, Sezione di Trieste*
[2]*Department of Physics and Arnold Sommerfeld Center for Theoretical Physics,*
Ludwig-Maximilians-Universität München, D-80333 München, Germany
(Dated: June 10, 2015)

We investigate the *classical* Rényi entropy S_n and the associated mutual information $\mathcal{I}_n$ in the Sherrington-Kirkpatrick (S-K) model, which is the paradigm model of mean-field spin glasses. First, using classical Monte Carlo simulations and analytical tools we investigate the S-K model on the n-sheets booklet. This is obtained by gluing together n independent copies of the model, and it is the main ingredient to construct the Rényi entaglement-related quantities. We find that at low temperature the S-K model is in a glassy phase, whereas at high temperature it exhibits paramagnetic behavior. Interestingly, the temperature of the paramagnetic-glassy transition depends non-trivially on the geometry of the booklet. At high-temperatures we provide the exact solution of the model exploiting the replica symmetry. This is the permutation symmetry among the fictitious replicas that are used in the replica trick to perform disorder averages. In the glassy phase the replica symmetry has to be broken. Using a generalization of the celebrated Parisi solution, we provide approximated results for S_n and $\mathcal{I}_n$, and for standard thermodynamic quantities. Both S_n and $\mathcal{I}_n$ exhibit a volume law in the whole phase diagram. We characterize analytically the behavior of the corresponding densities S_n/N and $\mathcal{I}_n/N$, in the thermodynamic limit. Remarkably, at the critical point $\mathcal{I}_n/N$ does not exhibit any crossing for different system sizes, in contrast with local spin models.

I. INTRODUCTION

Besides being ubiquitous in nature, disorder leads to several intriguing physical phenomena. Arguably, *spin glasses* represent one of the most prototypical examples of exotic behavior induced by disorder. While at any finite temperature disorder prevents the usual magnetic ordering, at low-enough temperatures these systems display a new type of "order". In the past decades an intense theoretical effort has been devoted to characterizing this spin glass order, the nature of the paramagnetic-glassy transition, and that of the associated order parameter[1-5].

All these issues can be thoroughly addressed in the Sherrington-Kirkpatrick (S-K) model[6,7], which is exactly solvable. The S-K model is a *classical* Ising model on the fully-connected graph of N sites, with quenched random interactions. Its hamiltonian reads

$$\mathcal{H} = -\sum_{1 \leq i < j \leq N} J_{ij} S_i S_j - h \sum_{1 \leq i \leq N} S_i. \qquad (1)$$

Here $S_i = \pm 1$ are classical Ising spins, h is an external magnetic field, and J_{ij} are uncorrelated (from site to site) random variables. The S-K model hosts a low-temperature glassy phase, which is separated from a high-temperature paramagnetic one by a second order phase transition. Despite its mean-field nature, the solution of the S-K model has been a mathematical challenge. Although it was proposed as an ansatz by Parisi[8] more than thirty years ago, its rigorous proof was obtained only recently[9]. Moreover, the solution exhibits several intricate features, such as lack of self-averaging[10], ultrametricity[11,12], and replica symmetry breaking[2,5]. The last refers to the breaking of the permutation symmetry among the fictitious replicas of the model, which are introduced to perform disorder averages (*replica trick*[13]). Finally, although the applicability of the S-K model to describe realistic spin glasses is still highly debated[14-16], there are recent proposals on how to realize it in cold-atomic gases[17,18], or in laser systems[19].

In the last decade entanglement-related quantities emerged as valuable tools to understand the physics of complex systems[20-23], both classical and quantum. For instance, at a conformally invariant critical point entanglement measures contain universal information about the underlying conformal field theory (CFT), such as the central charge[24-27]. For classical spin models a lot of attention has been focused on the *classical* Rényi entropy[28,29]. Given a bipartition of the system into two complementary subregions A and B, the classical Rényi entropy $S_n(A)$ (with $n \in \mathbb{N}$) is defined as

$$S_n(A) \equiv \frac{1}{1-n} \log \Big(\sum_{i_A \in \mathcal{C}_A} p_{i_A}^n \Big) \qquad (2)$$

Here $\mathcal{C}_A$ denotes the set of all the possible spin configurations in part A, whereas p_{i_A} is the probability of the configuration i_A. Alternatively, $S_n(A)$ can be obtained from the partition function of the model on an *ad hoc* defined "booklet" geometry (see section II for its definition). This consists of n independent and identical replicas (the booklet "sheets") of the model. These *physical* replicas are different from the *fictitious* ones used to perform the disorder average. Each sheet is divided into two parts A and B, containing N_A and N_B spins, respectively. The spins in part A of different sheets are constrained to be equal. It is convenient to introduce the booklet aspect ratio $0 \leq \omega \leq 1$ as

$$\omega \equiv \frac{N_A}{N}. \qquad (3)$$

Eq. (2) can also be used for quantum systems by interpreting p_{i_A} as the probability of finding part A in the *quantum* configuration i_A. In particular, for $n = 1$ Eq. (2) defines the subsystem Shannon entropy[30,31]. From $S_n(A)$, one defines the classical mutual information $\mathcal{I}_n(A, B)$ as

$$\mathcal{I}_n(A, B) \equiv S_n(A) + S_n(B) - S_n(A \cup B). \qquad (4)$$

For local models $\mathcal{I}_n$ obeys the area law[32] $\mathcal{I}_n(A) \propto \ell$, with ℓ the length of the boundary between A and B. Remarkably, for different ℓ, the ratio $\mathcal{I}_n/\ell$ exhibits a crossing at a second order phase transition[28], implying that it can be used as a diagnostic tool for critical behaviors. For conformally invariant critical models more universal information can be extracted from the area-law corrections of $\mathcal{I}_n$[29].

Recently, the study of the interplay between disorder and entanglement became a fruitful research area[33]. However, the behavior of entanglement-related quantities in glassy phases, and at glassy critical points, has not been explored yet (see Ref. [34] for some interesting results). Here we investigate both the classical Rényi entropy $S_n(A)$ and the mutual information $\mathcal{I}_n$ in the S-K model, using classical Monte Carlo simulations and analytical tools. We often restrict ourselves to the case with $n = 2$, as this is where numerical simulations are most efficient. As usual in disordered system, we focus on disorder-averaged quantities, considering $[S_n]$ and $[\mathcal{I}_n]$, with the brackets $[\cdot]$ denoting the average over different realizations of J_{ij} (cf. Eq. (1)).

We start discussing the thermodynamic phase diagram of the S-K model on the n-sheets booklet, as a function of temperature, and the aspect ratio ω (cf. Eq. (3)). We show that for any fixed ω the S-K model exhibits a low-temperature glassy phase, which is divided by the standard paramagnetic one at high temperatures by a critical point. Surprisingly, the critical temperature exhibits a non-trivial dependence on ω that we are able to determine analytically. In the high-temperature region the permutational symmetry among the replicas, both the physical and the fictitious ones, is preserved. This allows us to provide an exact analytic expression for the free energy of the model and several derived quantities, such as the internal energy. We compare our results with Monte Carlo simulations, finding perfect agreement. Oppositely, we provide evidence that in the low-temperature phase the replica symmetry is broken. For instance, we numerically observe that the replica-symmetric (RS) result for the internal energy is systematically lower than the Monte Carlo data, as in the standard S-K model[6,7]. This discrepancy becomes larger upon lowering the temperature.

Inspired by the Parisi scheme[35], we devise a systematic way of breaking the replica symmetry in successive steps. In our scheme we break only the symmetry among the fictitious replicas, preserving that among the physical ones. Although this appears natural, we are not able to provide a rigourous proof that this is the correct symmetry breaking pattern. In particular, we cannot exclude that the symmetry among the physical replicas has to be broken. As a consequence, our scheme should be regarded as an approximation, and not as an exact solution. We restrict ourselves to the one-level replica symmetry breaking (1-RSB). Surprisingly, we observe that the 1-RSB result for the internal energy is in excellent agreement with the Monte Carlo data for $\beta \lesssim 3$, whereas the RS approximation fails already at $\beta \approx 1$. This suggests that the 1-RSB ansatz captures correctly some aspects of the replica symmetry breaking.

Clear signatures of the replica symmetry breaking are observed in the behavior of $[S_2]$. First, since $[S_2]$ exhibits the
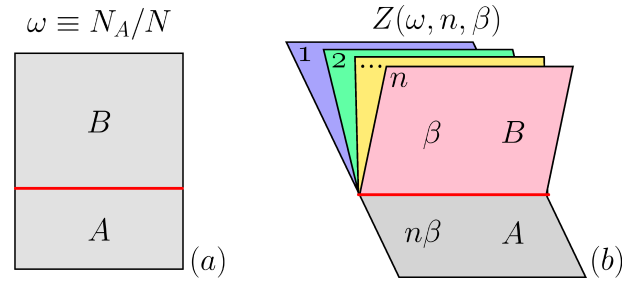

FIG. 1. The booklet geometry considered in this work. (a) The single sheet ("page") of the booklet: The N spins living on the sheet are divided into two groups A and B, containing N_A and N_B spins, respectively. Here $\omega \equiv N_A/N$ is the booklet ratio. (b) The n sheets are glued together to form the booklet. The spins in part B of the booklet pages are at inverse temperature β. The spins in part A are identified (see Eq. (9)). As a consequence, the effective temperature in part A is $n\beta$. $Z(A, n, \beta)$ denotes the partition function of the S-K model on the booklet.

volume law behavior $[S_2] \propto N$, we consider its density $[S_2]/N$. For finite-size systems, and for any ω, $[S_2]/N$ exhibits a maximum at infinite temperature, and it is a decreasing function of the temperature, as expected. Finite-size corrections are neglegible at high temperatures, whereas they increase upon lowering the temperature. In the paramagnetic phase we are able to determine the functional form of $[S_2]/N$ in the thermodynamic limit, using the replica-symmetric approximation. This perfectly matches the Monte Carlo data. At low temperatures deviations from the RS result are observed, reflecting the replica symmetry breaking. Remarkably, we observe that the one-step replica symmetry breaking (1-RSB) result S_2^{1-RSB}/N is in full agreement with the Monte Carlo data for $\beta \lesssim 3$, confirming what is observed for the internal energy.

Finally, we consider the Rényi mutual information $[\mathcal{I}_2]$. This obeys a volume law for any β and ω, in contrast with local spin models, where an area law is observed[32]. The corresponding density $[\mathcal{I}_2]/N$ vanishes in both the infinite-temperature and the zero-temperature limits. Surprisingly, $[\mathcal{I}_2]/N$ does not exhibit any crossing for different system sizes at the paramagnetic-glassy transition. This is in striking contrast with local spin models[28]. Interestingly, for any ω, $\mathcal{I}_2/N$ exhibits a maximum for $\beta \approx 1$. However, the position of this maximum is not simply related to the paramagnetic-glassy transition. Finally, at high temperature $[\mathcal{I}_2]/N$ is described analytically by the RS result $[\mathcal{I}_2]^{RS}/N$, whereas at low temperatures one has to include the effects of the replica symmetry breaking. Similar to $[S_2]$, we observe that the 1-RSB approximation $[\mathcal{I}_2^{1-RSB}]/N$, is in good agreement with the Monte Carlo data for $\beta \lesssim 3$.

The Article is organized as follows. In section II we introduce the classical Rényi entropy and the mutual information, reviewing their representation in terms of the booklet partition functions. In section III we present the structure of the solution of the S-K model on the booklet. Specifically, we discuss the replica trick, which is used to perform disorder averages, and the saddle point approximation in the thermodynamic limit. Section IV is concerned with the RS approx-

imation. Precisely, in subsection IV A we focus on the high-temperature region, where this pproximation becomes exact. In subsection IV B we discuss the structure of the RS ansatz in the low-temperature region. Section V is devoted to the 1-RSB approximation. In section VI we check the validity of both the RS and the 1-RSB results comparing with Monte Carlo simulations for the internal energy. Section VII and VIII discuss the classical Rényi entropy and the mutual information, respectively. Finally, we conclude in section IX.

II. THE BOOKLET CONSTRUCTION & AND THE CLASSICAL RÉNYI ENTROPY

Given a generic *classical* spin model at inverse temperature β, the classical Rényi entropy $S_n(A)$ is defined as[28,29]

$$S_n(A) \equiv \frac{1}{1-n} \log\left(\frac{Z(A,n,\beta)}{Z^n(\beta)} \right). \tag{5}$$

Here $Z(A,n,\beta)$ is the partition function of the model on the n-sheet booklet, whereas $Z(\beta)$ is the partition functions on the plane at inverse temperatures β. The booklet geometry is illustrated in Fig. 1. Each sheet is divided into two parts A and B (cf. Fig. 1 (a)). Then n copies of the system are "glued" together to form the booklet. The spins in part A of the different sheets are identified (cf. Fig. 1 (b)). While spins in parts B of the booklet are at inverse temperature β, the ones in A are at the effective temperature $n\beta$. Notice that a similar geometric construction[36] plays an important role in the mathematical proof of the Parisi ansatz.

Clearly, one has $S_n(A) \equiv 1/(n-1)\log(F(A,n,\beta)) - n\log(F(\beta))$, where $F(A,n,\beta) \equiv \log(Z(A,n\beta))$ and $F(\beta) \equiv \log(Z(\beta))$ are related (apart from a factor β) to the free energy of the model on the booklet and on the plane, respectively. The mutual information $\mathcal{I}_n(A,B,\beta)$ is defined[28,29] as

$$\mathcal{I}_n(A,B,\beta) \equiv \frac{1}{1-n} \log\left(\frac{Z(A,n,\beta)Z(B,n,\beta)}{Z^n(\beta)Z(n\beta)} \right), \tag{6}$$

where $Z(B,n,\beta)$ is obtained from $Z(A,n,\beta)$ by replacing A with B. Notice that the disorder-averaged mutual information $[\mathcal{I}_n]$ and the Rényi entropy $[S_n]$ are directly related to the so-called quenched-averaged free energy $[F(A,n,\beta)]$, which is the main quantity of interest in disordered systems[13].

For clean (i.e., without disorder) *local* spin models $\mathcal{I}_n$ obeys the boundary law

$$\mathcal{I}_n(A,B,\beta) = \alpha_n \ell + \mathcal{G}_n + \gamma_n, \tag{7}$$

with ℓ the length of the boundary between A and B, and α_n, γ_n two non-universal constants. Here $\mathcal{G}_n$ is the so-called geometric mutual information[29]. Interestingly, for critical systems $\mathcal{G}_n$ depends only on the geometry of A and B, and it is universal. In particular, for conformally invariant models $\mathcal{G}_n$ can be calculated using standard methods of conformal field theory (CFT), and it allows to numerically extract universal information about the CFT, such as the central charge[29].

III. THE SHERRINGTON-KIRKPATRICK (S-K) MODEL ON THE BOOKLET

Here we introduce the Sherrington-Kirkpatrick (S-K) model on the booklet. In subsection III A we define the model and its partition function. In subsection III B we discuss the replicated booklet construction that is used to calculate the disorder-averaged free energy $[F(\omega,n,\beta)]$. In section III C we consider the thermodynamic limit, using the saddle point approximation. We also introduce the overlap tensor, which contains all the information about the thermodynamic behavior of the model. The analytical formula for the replicated partition function (Eq. (20)), and the saddle point equations (Eqs. (23)(24)) for the overlap tensor are the main results of this section.

A. The model and its partition function

The Sherrington-Kirkpatrick (S-K) model[6,7] on the n-sheets booklet (cf. Fig. 1) is defined by the Hamiltonian

$$\mathcal{H} = -\sum_{r=1}^{n} \left\{ \sum_{i<j} J_{ij} S_i^{(r)} S_j^{(r)} - h \sum_{i=1}^{N} S_i^{(r)} \right\}. \tag{8}$$

Here $S_i^{(r)} = \pm 1$ are classical Ising spins, $r \in [1,n]$ labels the different sheets ("pages") of the booklet, $i \in [1,N]$ denotes the sites on each sheet, J_{ij} is the interaction strength, and h is an external magnetic field. Here we choose $h = 0$. The total number of spins in the booklet is nN. The first sum inside the brackets in Eq. (8) is over all the $N(N-1)/2$ pairs of spins in each sheet. Spins on different sheets do not interact. In each "sheet" of the booklet all the sites are divided into two groups $A \equiv \{1,\ldots,N_A\}$ and $B \equiv \{N_A+1,\ldots,N\}$, containing N_A and $N_B \equiv N - N_A$ sites, respectively. The spins living in part A and different sheets are identified, i.e., $\forall i \in A$ one has

$$S_i^{(r)} = S_i^{(r')} \quad \forall r, r'. \tag{9}$$

Since in each sheet all spins interact with each other, there is no notion of distance between different spins. Thus, physical observables should depend on the booklet geometry only through the ratio ω (cf. Eq. (3)).

In Eq. (8) the couplings $J_{ij} \in \mathbb{R}$ are uncorrelated (from site to site) quenched random variables. J_{ij} are the same in all the sheets of the booklet. Specifically, here J_{ij} are drawn from the gaussian distribution

$$P(J_{ij}) = \left(\frac{N}{2\pi} \right)^{1/2} \exp\left\{ -\frac{N}{2}\left(J_{ij} - \frac{J_0}{N} \right)^2 \right\}. \tag{10}$$

The mean and the variance of $P(\{J_{ij}\})$ are given as $[J_{ij}] = J_0/N$ and $[(J_{ij} - [J_{ij}])^2] = J^2/N$, respectively. The square brackets $[\cdot]$ denote the average over different realinzations of J_{ij}. Here we restrict ourselves to $J_0 = 0$ and $J = 1$. The factors N in Eq. (10) ensure a well-defined thermodynamic limit.

The partition function $Z(\omega, n, \beta, \{J\})$ of the S-K model on the booklet at inverse temperature $\beta \equiv 1/T$, and for fixed disorder realization $\{J_{ij}\}$, reads

$$Z(\omega, n, \beta, \{J\}) \equiv \mathrm{Tr}' \exp(-\beta \mathcal{H}) =$$
$$\mathrm{Tr}' \exp \left\{ \beta \sum_r \left(\sum_{i<j} S_i^{(r)} S_j^{(r)} - h \sum_{i=1}^N S_i^{(r)} \right) \right\}, \quad (11)$$

where $\mathrm{Tr}' \equiv \sum_{\{S_i\}}$ denotes the sum over all possible spin configurations. The prime in Tr' stresses that only spin configurations satisfying the constraint in Eq. (9) are considered. In the two limits $\omega = 0$ and $\omega = 1$ one recovers the standard S-K model. In particular, for $\omega = 0$, i.e., n disconnected sheets, one has $Z(0, n, \beta, \{J\}) = Z(\beta, \{J\})^n$, with $Z(\beta, \{J\})$ the partition function of the S-K model on the plane. On the other hand, for $\omega = 1$ it is $Z(1, n, \beta, \{J\}) = Z(n\beta, \{J\})$, i.e., the partition function of the S-K model at inverse temperature $n\beta$. The quenched averaged free energy $[F(\omega, n, \beta)]$, is defined as

$$[F(\omega, n, \beta)] \equiv -\frac{1}{\beta} \int \mathcal{D}\{J\} \log Z(\omega, n, \beta, \{J\}), \quad (12)$$

where $\int \mathcal{D}\{J\} \equiv \prod_{i<j} \int_{-\infty}^{+\infty} dJ_{ij} P(J_{ij})$.

At $\omega = 0$ and $\omega = 1$ the phase diagram of the S-K model in the thermodynamic limit is well established[4]. In particular, at $\omega = 0$ the model exhibits a standard paramagnetic phase in the high temperature region, whereas at low temperatures a glassy phase is present, with replica-symmetry breaking[4]. The two phases are divided by a second order phase transition at $\beta = \beta_c = 1$. The phase diagram for $\omega = 1$ is the same, apart from the trivial redefinition $\beta \to n\beta$. We anticipate here (see section IV B) that a similar scenario holds for generic ω. Specifically, the glassy replica-symmetry-broken phase at low temperatures survives for generic $0 < \omega < 1$, while at high temperature the model is paramagnetic. The critical point at $\beta = \beta_c(\omega)$, which marks the transition between the two phases, is a nontrivial function of the booklet ratio ω (see section IV C).

B. The replicated booklet and the overlap tensor

The disorder-averaged free energy $[F(\omega, n, \beta)]$ (cf. Eq. (12)) is obtained, using the standard replica trick[13], as

$$[F(\omega, n, \beta)] = \lim_{\alpha \to 0} \frac{[Z^\alpha(\omega, n, \beta)] - 1}{\alpha}. \quad (13)$$

Here $[Z^\alpha(\omega, n, \beta)]$ is the disorder-averaged partition function of $\alpha \in \mathbb{N}$ independent copies of the S-K model on the booklet. Precisely, $[Z^\alpha(\omega, n, \beta)]$ reads

$$[Z^\alpha(\omega, n, \beta)] = \int \mathcal{D}\{J\} \mathrm{Tr}' \exp \sum_{r,\gamma} \Big\{$$
$$\beta \sum_{i<j} J_{ij} S_i^{(r,\gamma)} S_j^{(r,\gamma)} + \beta h \sum_i S_i^{(r,\gamma)} \Big\}, \quad (14)$$

where the index $\gamma = 1, 2, \ldots, \alpha$ labels the different fictitious replicas introduced in Eq. (13), whereas r denote the physical replicas, as in Eq. (11). Clearly, physical and fictitious replicas do not interact. Notice that $Z^\alpha(\omega, n, \beta)$ can be thought of as the partition function of the S-K model on a "replicated" booklet.

Using Eq. (10), the disorder average in Eq. (14) can be performed explicitly, to obtain

$$[Z^\alpha(\omega, n, \beta)] = \mathrm{Tr}' \exp \sum_{r,\gamma} \Big\{$$
$$\frac{1}{N} \sum_{i<j} \Big(\frac{\beta^2}{2} \sum_{\gamma',r'} S_i^{(r,\gamma)} S_j^{(r,\gamma)} S_i^{(r',\gamma')} S_j^{(r',\gamma')}$$
$$+ \beta J_0 S_i^{(r,\gamma)} S_j^{(r,\gamma)} \Big) + \beta h \sum_i S_i^{(r,\gamma)} \Big\}. \quad (15)$$

In contrast with Eq. (14), physical and unphysical replicas are now coupled by a four-spin interaction. It is convenient to introduce the Hubbard-Stratonovich variables $q_{\gamma\gamma'}^{rr'}$ and m_γ^r. Following the spin glass literature[2], we dub $q_{\gamma\gamma'}^{rr'}$ the overlap tensor. In the standard S-K model (i.e., for $n = 1$) $q_{\gamma\gamma'}^{rr'}$ becomes a $\alpha \times \alpha$ matrix[7]. Eq. (15) now yields

$$[Z^\alpha(\omega, n, \beta)] = \exp \Big(\frac{\beta^2 N n \alpha}{4} \Big) \int \prod_{\substack{\gamma \leq \gamma' \\ r,r'}} dq_{\gamma\gamma'}^{rr'} \int \prod_{\gamma,r} dm_\gamma^r$$
$$\mathrm{Tr}' \exp \Big\{ - N\mathcal{K}(\{q, m\}) + \sum_i \mathcal{L}_i(\{q, m\}) \Big\}, \quad (16)$$

where we neglected subleading contributions $\mathcal{O}(1/N)$ in the thermodynamic limit. Here $\mathcal{K}(\{q, m\})$ is spin-independent and it reads

$$\mathcal{K}(\{q, m\}) \equiv \frac{\beta^2}{2} \Big(\sum_{\gamma < \gamma'} \sum_{r,r'} (q_{\gamma\gamma'}^{rr'})^2$$
$$+ \sum_\gamma \sum_{r<r'} (q_{\gamma\gamma}^{rr'})^2 \Big) + \frac{\beta}{2J_0} \sum_{\gamma r} (m_\gamma^r)^2. \quad (17)$$

On the other hand $\mathcal{L}_i(\{q, m\})$ depends on the spin degrees of freedom, and it is given as

$$\mathcal{L}_i(\{q, m\}) \equiv \beta^2 \sum_{\gamma < \gamma'} \sum_{r,r'} q_{\gamma\gamma'}^{rr'} S_i^{(r,\gamma)} S_i^{(r',\gamma')} +$$
$$\beta^2 \sum_\gamma \sum_{r<r'} q_{\gamma\gamma}^{rr'} S_i^{(r,\gamma)} S_i^{(r',\gamma)} + \beta \sum_{\gamma r} (m_\gamma^r + h) S_i^{(r,\gamma)}. \quad (18)$$

Interestingly, $\mathcal{L}_i$ describes a system of $n\alpha$ spins living in the replica space with the long-range interaction $q_{\gamma\gamma'}^{rr'}$, and a magnetic field $m_\gamma^r + h$. Notice that, while the first term in Eq. (18) is off-diagonal in the space of the fictitious replicas, the second one is diagonal. We anticipate here that the latter fully determines the behavior of the model in the paramagnetic phase (see section IV A).

Since in Eq. (16) spins on different sites are decoupled, one can perform the trace over the spins in parts A and B (see Fig. 1) independently, to obtain

$$[Z^\alpha(\omega, n, \beta)] = \int \prod_{\substack{\gamma \leq \gamma' \\ r,r'}} dq_{\gamma\gamma'}^{rr'} \int \prod_{\gamma,r} dm_\gamma^r \exp \Big\{ N \Big($$

$$\frac{\beta^2 n\alpha}{4} + \omega \log \mathrm{Tr}_A e^{\mathcal{L}} + (1-\omega) \log \mathrm{Tr}_B e^{\mathcal{L}} - \mathcal{K} \Big) \Big\}. \quad (19)$$

Here to lighten the notation we drop the dependence on the coordinate i and the arguments of $\mathcal{L}_i(\{q, m\})$ and $\mathcal{K}(\{q, m\})$. Tr_A and Tr_B denote the trace over the spin degrees of freedom living in parts A and B of the booklet. The subscript A in Tr_A is to stress that spins living in different physical replicas (i.e., for $r \neq r'$ in Eq. (18)) are identified (due to the booklet constraint in Eq. (9)), whereas they have to be treated as independent variables in performing Tr_B.

C. The saddle point approximation

In the thermodynamic limit, i.e., for $N, N_A \to \infty$, at fixed ratio $\omega \equiv N_A/N$, one can take the saddle point approximation in Eq. (19), which yields

$$[Z^\alpha(\omega, n, \beta)] \approx \exp \Big\{ N\alpha \Big(\frac{\beta^2 n}{4} - \frac{\mathcal{K}}{\alpha}$$

$$+ \frac{\omega}{\alpha} \log \mathrm{Tr}_A \exp(\mathcal{L}) + \frac{1}{\alpha}(1-\omega) \log \mathrm{Tr}_B \exp(\mathcal{L}) \Big) \Big\}. \quad (20)$$

The overlap tensor $q_{\gamma\gamma'}^{rr'}$ and m_γ^r are determined by solving the saddle point equations

$$\frac{\partial}{\partial q_{\gamma\gamma'}^{rr'}} \left(\omega \log \mathrm{Tr}_A e^{\mathcal{L}} + (1-\omega) \log \mathrm{Tr}_B e^{\mathcal{L}} \right) = q_{\gamma\gamma'}^{rr'} \quad (21)$$

$$\frac{\partial}{\partial m_\gamma^r} \left(\omega \log \mathrm{Tr}_A e^{\mathcal{L}} + (1-\omega) \log \mathrm{Tr}_B e^{\mathcal{L}} \right) = \frac{1}{J_0} m_\gamma^r. \quad (22)$$

It is enlightening to rewrite Eqs. (21) (22) as

$$q_{\gamma\gamma'}^{rr'} = \omega \langle S^{(r,\gamma)} S^{(r',\gamma')} \rangle_A + (1-\omega) \langle S^{(r,\gamma)} S^{(r',\gamma')} \rangle_B \quad (23)$$

$$\frac{1}{J_0} m_\gamma^r = \omega \langle S^{(r,\gamma)} \rangle_A + (1-\omega) \langle S^{(r,\gamma)} \rangle_B \quad (24)$$

where $\langle \mathcal{O} \rangle_{A(B)} \equiv (Z_{A(B)})^{-1} \mathrm{Tr}_{A(B)} \{ \mathcal{O} \exp(\mathcal{L}) \}$ with $Z_{A(B)} \equiv \mathrm{Tr}_{A(B)} \exp(\mathcal{L})$. Notice that Eq. (23) implies that $q_{\gamma\gamma}^{rr} = 1 \; \forall \gamma, r$. For $\omega = 0$ and $n = 1$, one recovers the saddle point equations for the standard SK model[2,4].

In order to calculate the free energy $[F(\omega, n, \beta)]$ one has to solve Eqs. (23) (24), take the analytic continuation $\alpha \in \mathbb{R}$, and, finally, the limit $\alpha \to 0$. (cf. Eq. (13)). Although it is possible to solve Eqs. (23) (24) numerically for any fixed $r, \alpha \in \mathbb{N}$, taking the analytic continuation $\alpha \in \mathbb{R}$ is a formidable task, since the dependence of $Z^\alpha(\omega, n, \beta)$ on α is in general too complicated. The strategy is usually to choose a specific form of the overlap tensor $q_{\gamma\gamma'}^{rr'}$ in terms of "few"
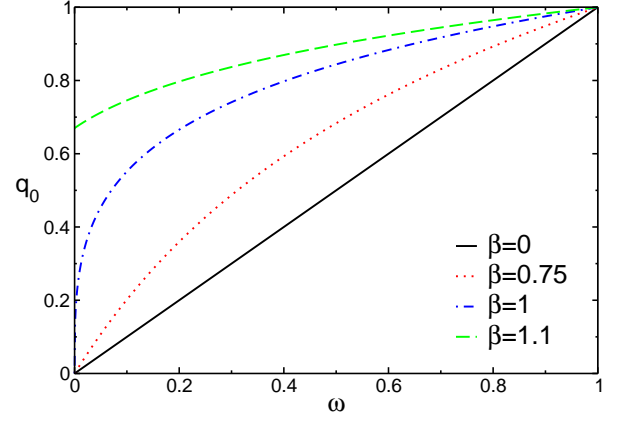

FIG. 2. The S-K model on the 2-sheets booklet with zero magnetic field in the paramagnetic phase: the solution q_0 of the saddle point equation (33) plotted as a function of the booklet aspect ratio ω and several values of the inverse temperature $\beta = 1/T$. At $\omega = 1$ one has $q_0 = 1, \forall \beta$. In the zero-temperature limit one has $q_0 \to 1, \forall \omega$. The straight line is the infinite temperature result.

parameters, which allows to perform the analytic continuation and the limit $\alpha \to 0$ exactly.

For the standard S-K model (i.e., for $n = 1$) the simplest parametrization is the replica-symmetric one (RS), which amounts to taking $q_{\gamma\gamma'}^{11} = q$. This relies on the observation that the fictitious replicas appear symmetrically in Eq. (14). Although the RS ansatz is correct at high temperatures, it fails in the glassy phase at low temperatures, where the permutational invariance within the replicas has to be broken[37]. the celebrated Parisi ansatz[35] provides a systematic scheme to break the replica symmetry in successive steps, and it allows to capture the the glassy behavior of the S-K model at low temperature. We anticipate (see section V for the details) that a similar scheme has to be used to describe the glassy phase of the S-K model on the booklet.

IV. THE REPLICA-SYMMETRIC (RS) ANSATZ

In this section we present the solution of the S-K model on the booklet, using the replica symmetric (RS) approximation. In subsection IV A we focus on the high temperature phase, where this approximation is exact, and the behavior of the model is fully determined by the diagonal part of the overlap tensor $q_{\gamma\gamma'}^{rr'}$ (see section III B for its definition). The generic structure of $q_{\gamma\gamma'}^{rr'}$ within the RS ansatz is discussed in subsection IV B. This allows us to determine the critical temperature of the paramagnetic-glassy transition.

A. The paramagnetic phase

Here we provide the exact analytical expression for the disorder-averaged free energy $[F_{para}(\omega, n, \beta)]$ in the paramagnetic non-glassy phase. We start discussing the infinite temperature limit (i.e., $\beta \to 0$), restricting ourselves

to zero magnetic field. Using Eq. (18), a standard high-temperature expansion yields $\mathrm{Tr}_A e^{\mathcal{L}} = 2^{\alpha} + \mathcal{O}(\beta^2)$ and $\mathrm{Tr}_B e^{\mathcal{L}} = 2^{n\alpha} + \mathcal{O}(\beta^2)$, implying

$$\langle S^{(r,\gamma)} S^{(r',\gamma')}\rangle_B = 2^{n\alpha}\delta_{\gamma,\gamma'}\delta_{r,r'} + \mathcal{O}(\beta^2) \quad (25)$$

$$\langle S^{(r,\gamma)} S^{(r',\gamma')}\rangle_A = 2^{\alpha}\delta_{\gamma,\gamma'} + \mathcal{O}(\beta^2). \quad (26)$$

Using Eq. (23), it is straightforward to obtain the infinite-temperature overlap tensor $q_{\gamma\gamma'}^{rr'}$ as

$$q_{\gamma\gamma'}^{rr'} = (1-\omega)\delta_{\gamma,\gamma'}\delta_{r,r'} + \omega\delta_{\gamma,\gamma'}. \quad (27)$$

Remarkably, $q_{\gamma\gamma'}^{rr'}$ becomes diagonal in both the indices γ, γ' and r, r', i.e., the physical and fictitious replica spaces. Using Eq (20) and Eq. (13), after performing the analytic continuation $\alpha \to 0$, one obtains

$$[F_{para}(\omega, n, \beta)] = N\Big\{ (n - \omega(n-1)) \log(2)$$
$$+ \frac{\beta^2}{4}(\omega^2(n^2-n)+n) \Big\} + \mathcal{O}(\beta^4). \quad (28)$$

It is natural to expect that for arbitrary $\beta \leq \beta_c$, with β_c the critical temperature of the paramagnetic-glassy transition, the overlap tensor $q_{\gamma\gamma'}^{rr'}$ remains diagonal. This suggests the ansatz

$$q_{\gamma\gamma'}^{rr'} = (1-q_0)\delta_{r,r'}\delta_{\gamma,\gamma'} + q_0\delta_{\gamma,\gamma'}. \quad (29)$$

with $q_0 \in \mathbb{R}$ a parameter. The ansatz (29) is formally obtained from Eq. (27) by replacing $\omega \to q_0$. Notice that one has $q_{\gamma\gamma}^{rr} = 1$, in agreement with Eqs. (23). Using Eq. (29), one obtains $\mathcal{L}_{para}$ (cf. Eq. (18)) as

$$\mathcal{L}_{para} = \beta^2 \frac{q_0}{2}\Big\{ \sum_{\gamma}\sum_{rr'} S^{(r,\gamma)} S^{(r',\gamma)} - n\alpha \Big\}. \quad (30)$$

After introducing the Hubbard-Stratonovich variables z_λ (with $\lambda = 1, \ldots, \alpha$), one can write

$$\mathrm{Tr}_B \exp(\mathcal{L}_{para}) =$$
$$\mathrm{Tr}_B \int \prod_\lambda Dz_\lambda \exp\Big(z_\lambda \beta \sqrt{q_0} \sum_r S^{(r,\lambda)} \Big), \quad (31)$$

where $\int Dz f(z) \equiv (2\pi)^{-1/2} \int \exp(-z^2/2) f(z)$. Notice that due to the square root in Eq. (31), one has the constraint $q_0 > 0$. Moreover, from Eq. (30) one obtains $\mathrm{Tr}_A \exp(\mathcal{L}) = 2^{n\alpha}$. The trace Tr_B in Eq. (31) can be performed explicitly. Using Eq. (20) and Eq. (13), one obtains the free energy $[F_{para}(\omega, n, \beta)]$ as

$$[F_{para}(\omega, n, \beta)] = N\Big\{ n\log(2) - \omega(n-1)\log(2)$$
$$+ \beta^2\Big(\frac{n}{4} - \frac{q_0^2}{4}(n^2-n) + \frac{\omega}{2}q_0 n^2 - q_0 n \Big)$$
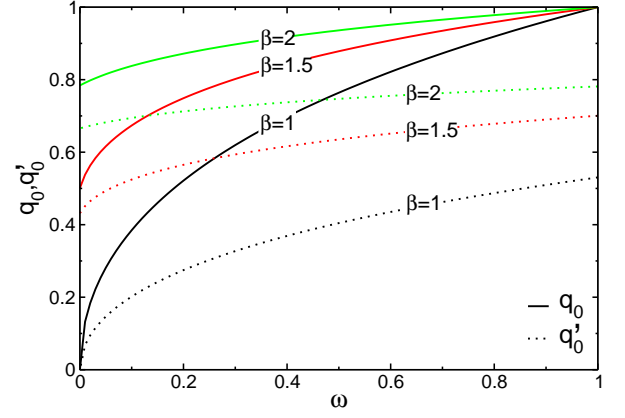$$+ (1-\omega)\log \int Dz \cosh^n(z\sqrt{q_0}\beta) \Big\}, \quad (32)$$

FIG. 3. The S-K model on the 2-sheets booklet with zero magnetic field. The overlap tensor in the replica-symmetric (RS) approximation (see Eq. (34)): the solutions q_0 and q_0' (shown as full and dotted lines, respectively) of the saddle point equations (A1)(A2) plotted as a function of the booklet aspect ratio ω, and inverse temperature $\beta = 1/T = 1, 3/2, 2$. At $\omega = 1$ one has that $q_0 = 1, \forall\beta$. In the limit $\beta \to \infty$ it is $q_0, q_0' \to 1, \forall\omega$.

where q_0 is determined by solving the saddle point condition $\partial[F_{para}(\omega, n, \beta)]/\partial q_0 = 0$. For the 2-sheets booklet (i.e., $n = 2$) this is given as

$$q_0 = \omega + (1-\omega)\tanh(\beta^2 q_0). \quad (33)$$

Alternatively, Eq. (33) can be obtained by substituting the ansatz (29) in Eqs. (23) (24).

Clearly, for two independent copies of the S-K model, i.e., $\omega = 0$, Eq. (33) gives $q_0 = 0$ for $\beta \leq 1$, whereas one has $q_0 \neq 0$ for $\beta > 1$. On the other hand, for $\omega = 1$ one has $q_0 = 1 \,\forall\beta$. For intermediate $0 < \omega < 1$, q_0 is plotted as a function of ω in Fig. 3. For $\beta = 0$ it is $q_0 = \omega$ (straight line in the Figure). In the low-temperature limit one has $q_0 \to 1$, for any ω. In particular, it is straightforward to check that $q_0 \approx 1 - 2(1-\omega)\exp(-2\beta^2)$ for $\beta \to \infty$.

B. The replica-symmetric (RS) approximation

In the replica-symmetric (RS) approximation one writes the overlap tensor $q_{\gamma\gamma'}^{rr'}$ as

$$q_{\gamma\gamma'}^{rr'} = (1-q_0)\delta_{r,r'}\delta_{\gamma,\gamma'} + q_0\delta_{\gamma,\gamma'} + (1-\delta_{\gamma,\gamma'})q_0'. \quad (34)$$

The first two terms in Eq. (34) are the same as in the para-magnetic phase (cf. Eq. (29)). The last term sets $q_{\gamma\gamma'}^{rr'} = q_0'$ $\forall\gamma \neq \gamma'$ and $\forall r, r'$. Clearly, $q_{\gamma\gamma'}^{rr'}$ is symmetric in both the physical and fictitious replica spaces. We do not have any rigorous argument to justify the ansatz (34), besides its simplicity. However, we numerically observe that it captures quite accurately the behavior of the model, at least around the paramagnetic-glassy transition (see section VI for the comparision with Monte Carlo data).

Using Eq. (34) and Eqs. (13)(20) one obtains the replica-symmetric approximation for the free energy $[F_{RS}(\omega, n, \beta)]$

as

$$[F_{RS}(\omega, n, \beta)] =$$
$$\lim_{\alpha \to 0} \left\{ N \left[\frac{\beta^2}{4} n - \frac{\beta^2}{4} \left((q_0^2 - (q_0')^2) n^2 - q_0^2 n \right) \right. \right.$$
$$+ \frac{1-\omega}{\alpha} \log \text{Tr}_B \exp(\mathcal{L}_{RS})$$
$$\left. \left. + \frac{\omega}{\alpha} \log \text{Tr}_A \exp(\mathcal{L}_{RS}) \right] \right\}, \quad (35)$$

where $\mathcal{L}_{RS}$ is obtained by substituting Eq. (34) in Eq. (18), which yields

$$\mathcal{L}_{RS} = \frac{q_0'}{2} \beta^2 \sum_{\gamma\gamma'} \sum_{rr'} S^{(r,\gamma)} S^{(r',\gamma')}$$
$$+ \frac{q_0 - q_0'}{2} \beta^2 \sum_{\gamma} \sum_{rr'} S^{(r,\gamma)} S^{(r',\gamma')} - \frac{q_0}{2} \beta^2 n\alpha. \quad (36)$$

To calculate the last two terms in Eq. (35) one has to introduce two auxiliary Hubbard-Stratonovich variables z, z', similar to the paramagnetic phase (cf. section IV A). Thus, after performing the trace over the spin variables, in the limit $\alpha \to 0$, one obtains

$$\log \text{Tr}_B \exp(\mathcal{L}_{RS}) = -\frac{q_0}{2} \beta^2 n\alpha + n\alpha \log(2) \quad (37)$$
$$+ \alpha \int Dz \log \int Dz' H_{RS}^n(z, z'),$$

$$\log \text{Tr}_A \exp(\mathcal{L}_{RS}) = -\frac{q_0}{2} \beta^2 n\alpha + \alpha \log(2) \quad (38)$$
$$+ \alpha \int Dz \log \int Dz' H_{RS}(nz, nz'),$$

where $H_{RS}(z, z') \equiv \cosh(\beta z \sqrt{q_0'} + \beta z' \sqrt{q_0 - q_0'})$. Notice that because of the square roots in the definition of $H_{RS}(z, z')$, one has the constraint $0 \le q_0' \le q_0 \le 1$.

In Eqs. (37)(38) q_0, q_0' satisfy the saddle point conditions $\partial [F_{RS}(\omega, n, \beta)]/\partial q_0 = \partial [F_{RS}(\omega, n, \beta)]/\partial q_0' = 0$ (cf. Eqs. (A1)(A2) for their form for $n = 2$). The resulting q_0 and q_0' are plotted in Fig. 3 (full and dotted lines, respectively) as function of ω and for several values of β. Clearly, for any β one has $q_0 = 1$ in the limit $\omega \to 1$. Also, in the zero-temperature limit $\beta \to \infty$ one has that $q_0 \to 1$ and $q_0' \to 1$, for any ω. Moreover, a simple calculation yields

$$q_0 = 1 - (1-\omega) \sqrt{\frac{2}{\pi}} \frac{1}{\beta} \exp\left(-\frac{1}{\pi} - \sqrt{\frac{2}{\pi}} \beta \right) + \dots \quad (39)$$

$$q_0' = 1 - \frac{1}{\sqrt{2\pi}\beta} - \frac{1}{2\pi\beta^2} + \mathcal{O}(\beta^{-3}), \quad (40)$$

with the dots denoting exponentially suppressed terms in the limit $\beta \to \infty$. Interestingly, from Eq. (39) one has that $q_0 \to 1$ exponentially in the limit $\beta \to \infty$, as in the paramagnetic phase (cf. section IV A), whereas $q_0' - 1 \propto 1/\beta$, similar to the standard SK model[4].
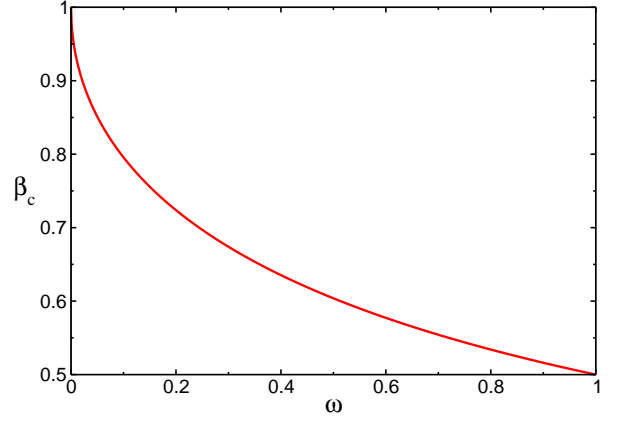

FIG. 4. The critical temperature $\beta_c \equiv 1/T_c$ of the paramagnetic-glassy transition for the S-K model on the 2-sheets booklet (see Fig. 1) with zero magnetic field: β_c as a function of the booklet ratio $\omega \equiv N_A/N$. Here β_c is obtained from the replica-symmetric (RS) approximation. Notice that $\beta_c = 1$ and $\beta_c = 1/2$ for $\omega = 0$ and $\omega = 1$, respectively.

C. The paramagnetic-glassy transition

Using the replica-symmetric ansatz Eq. (34) one can determine the critical temperature β_c of the paramagnetic-glassy transition. Near the glassy transition one should expect $q_0' \to 0$, whereas q_0 should remain finite (see section IV A). By expanding $[F_{RS}(\omega, n, \beta)]$ (cf. Eq (35)) for small q_0', and keeping only terms up to $\mathcal{O}((q_0')^2)$, one obtains a standard Landau theory. Thus, β_c is obtained by imposing that the coefficient of the quadratic term $q_0'^2$ changes sign. This leads to the equation

$$\exp(-4q_0\beta_c^2) + 2\exp(-2q_0\beta_c^2) = \frac{1 - 4\beta_c^2}{4\beta_c^2\omega - 1}, \quad (41)$$

where q_0 is obtained by solving the high-temperature saddle point equation (33). The resulting β_c is plotted in Fig. 4 as a function of ω.

V. THE ONE-STEP REPLICA-SYMMETRY-BREAKING (1-RSB) APPROXIMATION

In this section we go beyond the replica-ymmetric approximation, including some of the effects of the replica symmetry breaking. More specifically, here we discuss the one-step replica symmetry breaking (1-RSB) approximation. The overlap tensor $q_{\gamma\gamma'}^{rr'}$ now reads

$$q_{\gamma\gamma'}^{rr'} = (1 - q_0)\delta_{\gamma,\gamma'}\delta_{r,r'} + q_0\delta_{\gamma,\gamma'} + (1 - \delta_{\gamma,\gamma'})q', \quad (42)$$

which is formally equivalent to the RS ansatz in Eq. (34), apart from the trivial redefinition $q_0' \to q'$. However, in contrast with Eq. (34), where $q_0' \in \mathbb{R}$ is a number, here q' is a matrix. Inspired by the Parisi scheme for the standard S-K model[35],

FIG. 5. The S-K model on the 2-sheets booklet with zero magnetic field and booklet ratio $\omega = 1/2$ (see Fig. 1): The internal energy per spin U/N as a function of the inverse temperature β. The triangles, squares, and rhombi, denote the Monte Carlo data for a booklet with $N = 32, 64, 128$ spins per sheet. The plus symbols are the extrapolations to the thermodynamic limit $N \to \infty$, at fixed ω. The dash-dotted line is the analytical result U_{RS}/N obtained using the replica-symmetric (RS) approximation. The horizontal dotted line is the exact zero-temperature result $U/N \approx -1.52642$.

we choose

$$
q' = \begin{cases} q'_1 & \text{if } \lfloor \gamma/m_1 \rfloor = \lfloor \gamma'/m_1 \rfloor \\ q'_0 & \text{otherwise} \end{cases} \tag{43}
$$

where $q'_0, q'_1 \in \mathbb{R}$, $m_1 \in \mathbb{N}$, and $\lfloor \cdot \rfloor$ denotes the floor function. Notice that the off-diagonal elements of q' (i.e., for $\gamma \neq \gamma'$) do not depend on r, r', meaning that, although the permuta-

tional symmetry between the fictitious replicas is broken, the symmetry among the physical ones is preserved. The choice in Eq. (43) corresponds to a simple block-diagonal structure for q': the matrix elements of the $m_1 \times m_1$ diagonal blocks of q' are set to q'_1, whereas all the off-diagonal elements are set to q'_0. As for the replica-symmetric ansatz in Eq. (34), we do not have any rigorous argument to justify Eq. (43) (see section (VI), however, for numerical results).

The effective interaction $\mathcal{L}_{1\text{-}RSB}$ (cf. Eq. (18)) in the replica space is obtained by substituting Eq. (42) in Eq. (18). This yields

$$
\mathcal{L}_{1\text{-}RSB}/\beta^2 = -\frac{q_0}{2} n\alpha - \frac{q'_1 - q_0}{2} \sum_{\sigma=1}^{\alpha/m_1} \sum_{\gamma \in B_\sigma} \Big(\sum_r S^{(r,\gamma)} \Big)^2
$$
$$
+ \frac{q'_0}{2} \Big(\sum_{\gamma,r} S^{(r,\gamma)} \Big)^2 - \frac{q'_0 - q'_1}{2} \sum_{\sigma=1}^{\alpha/m_1} \Big(\sum_{\gamma \in B_\sigma, r} S^{(r,\gamma)} \Big)^2, \tag{44}
$$

where we defined $B_\sigma \equiv [\sigma m_1, (\sigma+1)m_1)$ with $\sigma \in \mathbb{N}$. It is convenient to introduce the Hubbard-Stratonovich variables $z, z_\sigma, z_{\sigma,\gamma}$ (one for each term in Eq. (44)). One then obtains

$$
\log \text{Tr}' \exp(\mathcal{L}_{1\text{-}RSB}) = -\frac{q_0}{2} \beta^2 n\alpha
$$
$$
+ \log \text{Tr}' \int Dz \prod_\sigma \int Dz_\sigma \prod_{\gamma \in B_\sigma} \int Dz_{\sigma,\gamma} \prod_r \exp \Big\{
$$
$$
\beta \Big(z\sqrt{q'_0} + z_{\sigma,\gamma}\sqrt{q_0 - q'_1} + z_\sigma \sqrt{q'_1 - q'_0} \Big) S^{(r,\gamma)} \Big\}. \tag{45}
$$

The trace over the spin variables in Eq. (45) can be now performed explicitly. Finally, one obtains the 1-RSB approximation for the free energy $[F_{1\text{-}RSB}(\omega, n, \beta)]$ as

$$
[F_{1\text{-}RSB}(\omega, n\beta)]/N = (\omega + (1-\omega)n)\log(2) + \frac{n}{4}\beta^2 \Big(1 + nq'^2_0 - n(m_1 - 1)(q'^2_1 - q'^2_0) - (n-1)q_0^2 - 2q_0 \Big)
$$
$$
+ \int Dz \Big\{ \frac{\omega}{m_1} \log \int Dz' \Big\{ \int Dz'' H^n_{1\text{-}RSB}(z, z', z'') \Big\}^{m_1} + \frac{1-\omega}{m_1} \log \int Dz' \Big\{ \int Dz'' H_{1\text{-}RSB}(nz, nz', nz'') \Big\}^{m_1} \Big\}, \tag{46}
$$

where we defined $H_{1\text{-}RSB}(z, z', z'')$ as

$$
H_{1\text{-}RSB}(z, z', z'') \equiv \cosh(z\beta\sqrt{q'_0}
$$
$$
+ z''\beta\sqrt{q_0 - q'_1} + z'\beta\sqrt{q'_1 - q'_0}). \tag{47}
$$

Similar to the replica-symmetric situation (see section IV B), from Eq. (47) one has the constraint $0 \leq q'_0 \leq q'_1 \leq q_0 \leq 1$. The parameters q_0, q'_0, q'_1, m_1 are obtained by solving the saddle point equations (A7)(A8)(A9) (A10). One should remark that, although formally m_1 is an integer, one obtains $m_1 \in \mathbb{R}$ from the saddle point equations. Clearly, the replica-symmetric result $[F_{RS}(\omega, n, \beta)]$ (cf. Eq. (35)) is recovered from Eq. (46) in the limit $q'_1 = q'_0$, while the free energy in

the paramagnetic phase $[F_{para}(\omega, n, \beta)]$ (cf. Eq. (32)) corresponds to $q'_1 = q'_0 = 0$.

VI. MONTE CARLO RESULTS: THE INTERNAL ENERGY

In this section we numerically confirm the analytical results of section IV. We discuss Monte Carlo (MC) data for the S-K model on the 2-sheets booklet with zero external magnetic field. We focus on the internal energy $U(\omega, n, \beta)$

$$
U(\omega, n, \beta) \equiv -\frac{\partial}{\partial \beta}[\log(Z(\omega, n, \beta))]. \tag{48}
$$

Fig. 5 plots the MC data for $U(\omega, 2, \beta)$ versus the inverse temperature β, for $\omega = 1/2$. The circles, squares, and triangles are the MC results for different sizes, i.e., number of spins per sheet, $N = 32, 64, 128$. The vertical dotted line is the critical temperature $\beta_c \approx 0.6$ of the paramagnetic-glassy transition (cf. Fig. 4). In the high-temperature region finite size effects are small, and already for $N = 64$ the MC data are indistinguishable from the thermodynamic limit. Oppositely, stronger scaling corrections are visible in the low-temperature phase at $\beta > \beta_c$. The plus symbols in Fig. 5 are the numerical extrapolations in the thermodynamic limit. These are obtained by fitting the finite size MC data to the ansatz $U/N = u_\infty(\omega, \beta) + c/N^\phi$, where u_∞ is energy density in the thermodynamic limit, c a fitting parameter, and ϕ the exponent of the scaling corrections. In our fits we fix $\phi = 2/3$, which is the exponent governing the finite-size corrections of U/N in the standard S-K model[38,39].

The dash-dotted line in Fig. 5 is the analytical result U_{RS} obtained using the replica-symmetric (RS) approximation (see section IV B). Using Eq. (35) and Eq (48), U_{RS} is obtained as

$$U_{RS} = -N\beta(1 + q_0^2 - 2q_0'^2).\qquad(49)$$

Here q_0, q_0' are solutions of the saddle point equations Eqs. (A1) (A2). Notice that U_{RS} depends on ω only through q_0, q_0'. From Fig. 5 one has that, while U_{RS} is in perfect agreement with the numerics for $\beta \approx \beta_c$, deviations appear in the low-temperature region. Notice that already at $\beta \gtrsim 1$, U_{RS} is incompatible with the data. Moreover, these deviations increase upon lowering the temperature. This has to be attributed to the replica symmetry breaking happening in the glassy phase. Finally, since in the limit $\beta \to \infty$ all the physical replicas are in the same state, one should expect that $u_\infty(\omega, \beta) \to n\tilde{u}_\infty$ (horizonthal line in Fig. 5), with $\tilde{u}_\infty = -0.76321...$[35,40] the zero-temperature internal energy density of the S-K model on the plane. Surprisingly, this behavior is already observed in the MC data at $\beta \approx 3$, whereas it is not captured correctly by the RS approximation.

The behavior of U/N for $\omega \neq 1/2$ is investigated in Fig. 6, plotting U/N as a function of β and $\omega = 0, 1/4, 1/2, 3/4, 1$. The plus symbols are the MC data extrapolated to the thermodynamic, at fixed ω. Similar to Fig. 6, the extrapolations are done assuming $U/N(\omega, n, \beta) = u_\infty(\omega, n, \beta) + c/N^\phi$, with $\phi = 2/3$ irrespective of ω. The stars in Fig. 6 are the critical values U_c/N at the paramagnetic-glassy transition. Specifically, here β_c is obtained by numerically solving Eq. (41). The lines in Fig. 6 denote U_{RS} (cf. Eq. (49)). At high temperature, and for generic n and ω, Eq. (28) and Eq. (48) give

$$U_{RS} = -N\frac{\beta}{2}(\omega^2(n^2 - n) + n) + \mathcal{O}(\beta^2),\qquad(50)$$

i.e., a linear behavior of U/N as a function of β. For $\omega = 0$ and $\omega = 1$ this behavior is exact up to the critical point at $\beta = \beta_c$, meaning that the higher orders $\mathcal{O}(\beta^2)$ in Eq. (50) are zero. This is only an approximation at intermediate $0 < \omega < 1$. Both the behaviors in Eq. (49) and Eq. (50) are clearly confirmed in Fig. 6.

However, the RS result is not correct for $\beta > \beta_c$, where the replica symmetry breaking has to be taken into account.
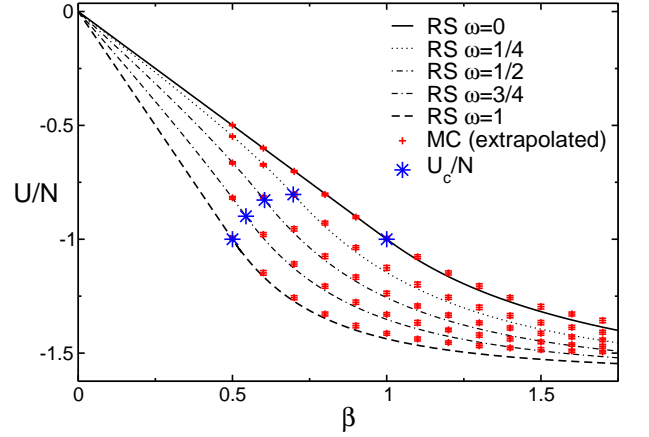

FIG. 6. The S-K model on the 2-sheets booklet and zero magnetic field: The internal energy per spin U/N in the thermodynamic limit. The symbols are the Monte Carlo data extrapolated to the thermodynamic limit $N \to \infty$, at fixed booklet ratio ω (see Fig. 1). U/N is plotted as a function of inverse temperature β and for $\omega = 0, 1/4, 1/2, 3/4, 1$. The lines are the analytical results U_{RS} obtained using the replica-symmetric (RS) approximation. The stars denote the value of U_c/N at the paramagnetic-glassy transition.
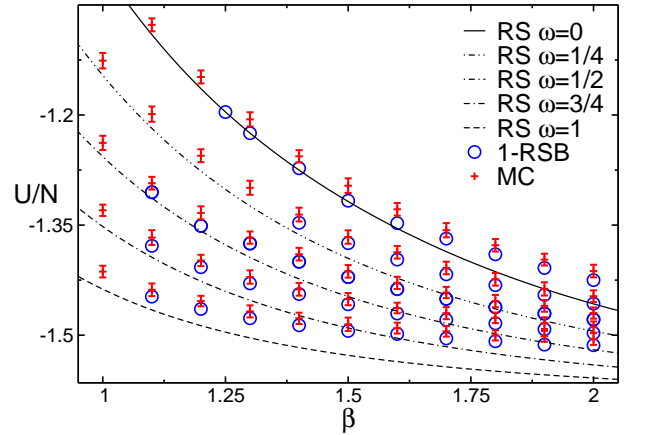

FIG. 7. The S-K model on the 2-sheets booklet with zero magnetic field: The internal energy per spin U/N in the thermodynamic limit plotted as a function of inverse temperature β. The plus symbols are the same Monte Carlo data as in Fig. 6. The lines denote U/N in the replica-symmetric (RS) approximation (same as in Fig. 6). The circles are the results in the one-step replica symmetry breaking (1-RSB) approximation.

The effects of the replica symmetry breaking are more carefully discussed in Fig. 7, focusing on the low temperature phase at $1 \leq \beta \leq 2$. The plus symbols and the lines are the same as in Fig. 6. The circles denote the internal energy per spin $U_{1\text{-}RSB}/N$ as obtained using the 1-step replica symmetry breaking (1-RSB) approximation (see section V). Specifically, from Eq. (46) and Eq. (48), for $n = 2$ a straightforward calculation gives

$$U_{1\text{-}RSB} = -N\beta(1 + q_0^2 + 2q_1'^2(m_1 - 1) - 2q_0'^2 m_1),\quad(51)$$

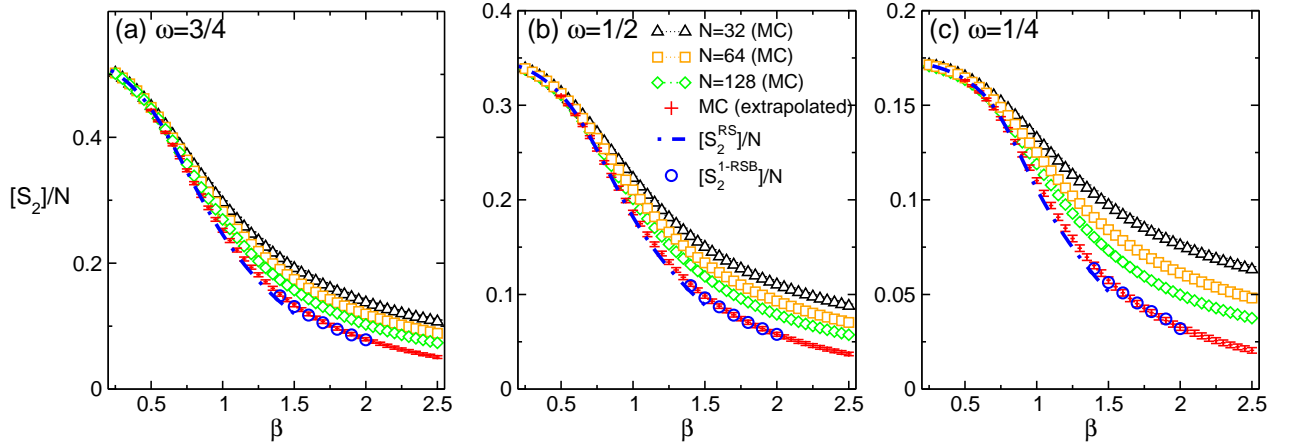where $q_0, q_0', q_1', m_1 \in \mathbb{R}$ are solutions of the saddle point

FIG. 8. The classical disorder-averaged Renyi entropy per spin $[S_2(\omega)]/N$ in the S-K model on the 2-sheets booklet with zero magnetic field: $[S_2(\omega)]/N$ as a function of the inverse temperature β. The different panels correspond to different booklet aspect ratios $\omega = 3/4, 1/2, 1/4$ (see Fig. 1). The triangles, squares and rhombi denote the Monte Carlo results for booklets with $N = 32, 64, 128$ spins per sheet. The plus symbols are the numerical extrapolations to the thermodynamic limit. The dash-dotted lines are the analytical results in the replica-symmetry (RS) approximation. The circles are the analytical results obtained using the one-step replica symmetry breaking (1-RSB) ansatz.

equations (A7)-(A10). Clearly, Eq. (51) implies $U_{1\text{-}RSB} \rightarrow U_{RS}$ for $q_1' \rightarrow q_0'$, as expected. Moreover, for $\beta \approx \beta_c$ one has $q_1' \approx q_0' \approx 0$, implying that $U_{1\text{-}RSB} \approx U_{RS}$, i.e. the effects of the replica symmetry breaking are negligible near the critical point. Interestingly, at low temperatures, where the RS approximation fails (see Fig. 6), $U_{1\text{-}RSB}$ is in good agreement with the Monte Carlo data, at least up to $\beta \approx 2$. This allows us to conclude that, although the 1-RSB ansatz (cf. Eq. (42)) is not correct for $\beta \rightarrow \infty$, it captures some of the effects of the replica symmetry breaking.

VII. THE CLASSICAL RÉNYI ENTROPIES

We now turn to discuss the behavior of the disorder-averaged classical Rényi entropies (cf. Eq. (5)). Here we restrict ourselves to the second Rényi entropy $[S_2]$. Due to the mean-field nature of the S-K model (cf. Eq. (8)), there is no well defined boundary between the two parts A and B of the system (unlike in local spin models). This suggests the volume-law behavior $[S_2] \propto N$ for all temperatures. Thus, it is natural to consider the entropy per spin $[S_2]/N$.

The Monte Carlo data for $[S_2]/N$ are shown in Fig. 8 plotted versus the inverse temperature $0.25 \leq \beta \leq 2.5$. Some details on the Monte Carlo method used to calculate $[S_2]$ are provided in Appendix B. The different panels correspond to the booklet ratios $\omega = 3/4, 1/2, 1/4$ (see Fig. 1). In all panels the triangles, squares, and rhombi correspond to booklets with $N = 32, 64, 128$ spins per sheet. Clearly, finite size effects are present, which increase upon lowering the temperature, as expected. In order to obtain $[S_2]/N$ in the thermodynamic limit we fit the data to the ansatz $[S_2]/N = s_2(\omega) + c'(\omega)/N^{\phi'}$, where $s_2(\omega)$ is the entropy per spin in the thermodynamic limit, c' a constant, and ϕ' the exponent of the finite-size corrections. The plus symbols in Fig. 8 are the results of the fits. We should mention that the fits give $\phi' \approx 2/3$, which

is the exponent of the scaling corrections of the free energy in the standard S-K model. This is not surprising, since $[S_2]$ is obtained as the difference $[S_2] \equiv [F(0, 2, \beta) - F(\omega, 2, \beta)]$ (cf. Eq. (5)). Clearly, from Fig. 8 one has that in the thermodynamic limit $[S_2]/N$ is finite for any β, confirming the expected volume law behavior. Moreover, $[S_2]/N$ exhibits a maximum in the infinite-temperature limit $\beta \rightarrow 0$. The height of this maximum is a decreasing function of ω (compare the panels (a)(b)(c) in Fig. 8).

The dash-dotted line denotes the analytical result $[S_2^{RS}]$ obtained within the RS approximation (see section IV B). More precisely, $[S_2^{RS}]/N$ is obtained from Eq. (5) and the expression for the free energy $[F_{RS}]$ (cf. Eq. (35)). Notice that in the high-temperature limit $\beta \rightarrow 0$, where the RS approximation is exact, Eq. (5) and Eq. (32) give

$$[S_2^{RS}] = \omega \log(2) - \frac{\beta^2}{4}\omega^2 + \mathcal{O}(\beta^3). \tag{52}$$

From Fig 8 one has that the extrapolated MC data are in quantitative agreement with $[S_2^{RS}]/N$ for $\beta \lesssim 1.5$, whereas strong deviations are observed at lower temperatures (not shown in the Figure). A better approximation for $[S_2]/N$ at low temperatures is obtained by including the effects of the replica symmetry breaking. The circles in Fig. 8 denote the one-step replica symmetry breaking result $[S_2^{1\text{-}RSB}]/N$ (see section V), which is obtained from Eq. (5) Eq. (46). Remarkably, $[S_2^{1\text{-}RSB}]/N$ is in excellent agreement with the Monte Carlo extrapolations for $\beta \lesssim 2$.

VIII. THE CLASSICAL RÉNYI MUTUAL INFORMATION

Here we focus on the behavior of the Renyi mutual information $[\mathcal{I}_2]$. Similar to $[S_2]$, the mutual information exhibits the volume law $[\mathcal{I}_2] \propto N$. This is in contrast with local models, where $[\mathcal{I}_n]$ for any n by construction obeys an area law
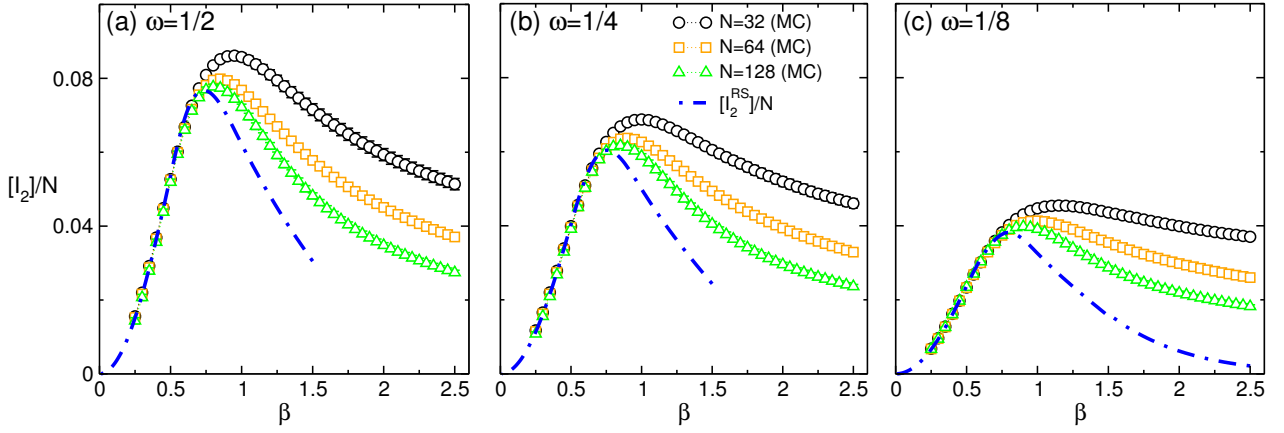
FIG. 9. The classical disorder-averaged mutual information per spin $[\mathcal{I}_2]/N$ in the S-K model on the 2-sheets booklet with zero magnetic field: $[\mathcal{I}_2]/N$ versus the inverse temperature β. The different panels correspond to different booklet ratios $\omega = 1/2, 1/4, 1/8$ (see Fig. 1). The same scale is used on both axes in all panels. The symbols are the Monte Carlo data for systems with $N = 32, 64, 128$ spins per sheet. The dash-dotted line is the analytical result in the replica-symmetric (RS) approximation.

at all temperatures. Here we consider the mutual information per spin $[\mathcal{I}_2]/N$.

Figure 9 plots $[\mathcal{I}_2]/N$ versus $0 \leq \beta \leq 2.5$ and $\omega = 1/2, 1/4, 1/8$ (panels from left to right in the Figure). Notice that by definition (cf. Eq. (6)) $[\mathcal{I}_n(\omega)] = [\mathcal{I}_n(1 - \omega)]$. Circles, squares, and triangles are Monte Carlo data for $N = 32, 64, 128$. In the high-temperature region $[\mathcal{I}_2]$ exhibits a vanishing behavior. Finite size effects are "small". Using Eq. (28) it is straightforward to derive the high-temperature behavior of $[\mathcal{I}_n]$ as

$$[\mathcal{I}_n] = \frac{N\beta^2}{2}\omega(1 - \omega)n + \mathcal{O}(\beta^4). \qquad (53)$$

Moreover, $[\mathcal{I}_2]/N$ increases upon lowering the temperature, up to $\beta \approx 1$, where it exhibits a maximum. The height of this maximum decreases as a function of ω. Its position is not simply related to the paramagnetic-glassy transition in the standard S-K model. This is not surprising as $[\mathcal{I}_n]$ is constructed by combining the partition functions on booklets with different aspect ratios $\omega, 1 - \omega, \omega = 0$, and $\omega = 1$ (cf. Eq. (6)), and the critical temperature of the paramagnetic-glassy transition is a non trivial function of ω (see Fig. 4). Furthermore, the data for $[\mathcal{I}_2]/N$ at different system sizes do not exhibit any crossing. This is in sharp contrast with local models[28], where $\mathcal{I}_n/L$ exhibits a crossing at a second order phase transition. The dash-dotted line in Fig. 9 is the analytical result obtained using the replica symmetric (RS) approximation (see section IV B). Formally, this is obtained using Eq (6) and Eq. (35), and it is in perfect agreement with the MC data in the whole paramagnetic phase.

Interestingly, at low temperatures $[\mathcal{I}_2]/N$ exhibits strong finite-size corrections, and significant deviations from the RS result. In order to extract the thermodynamic behavior of $[\mathcal{I}_2]/N$ we fit the MC data to

$$\frac{[\mathcal{I}_2]}{N} = a + \frac{b}{N^{\phi''}}, \qquad (54)$$

where we fix $\phi'' = 2/3$. The results of the fits are shown in Fig. 10 (circles, squares, and triangles). Remarkably, the RS approximation (dash-dotted lines) is in good agreement with the extrapolations up to $\beta \lesssim 1.5$, whereas deviations occur at lower temperatures (not shown in the figure). For $\omega = 1/8$, the numerical results exhibit deviations from the RS result already at $\beta \gtrsim 1$. These deviations have to be attributed to the physics of the replica symmetry breaking. The full rhombi in Fig. 10 denote the one-step replica symmetry breaking result $[\mathcal{I}_2^{1\text{-}RSB}]$, which is obtained using Eq. (6) and Eq. (46)). The agreement between $[\mathcal{I}_2^{1\text{-}RSB}]$ and the Monte Carlo data is perfect up to $\beta \lesssim 2$.

IX. SUMMARY AND CONCLUSIONS

We investigated the *classical* Rényi entropy S_n and the mutual information $\mathcal{I}_n$ in the Sherrington-Kirkpatrick (S-K) model, which is the paradigm model of mean-field spin glasses. We focused on the quenched averages $[S_n]$ and $[\mathcal{I}_n]$, with the brackets $[\cdot]$ denoting the average over different disorder realizations. Specifically, here $[S_n]$ and $[\mathcal{I}_n]$ were obtained from suitable combinations of the partition functions of the S-K model on the n-sheets booklet (cf. Fig. 1). This is constructed by "gluing" together n independent replicas ("sheets") of the model. On each replica the spins are divided into two groups A and B, containing N_A and N_B spins respectively. The spins in part A of the different sheets are identified. Due to the mean-field nature of the model, physical quantities depend on the bipartition only through the aspect ratio $\omega \equiv N_A/N$.

We first investigated the phase diagram of the S-K model on the 2-sheets booklet as a function of ω and the inverse temperature β. We considered the situation without external magnetic field ($h = 0$ in Eq. (1)). For any ω, in the thermodynamic limit, the model exhibits a glassy phase for low enough temperatures and a standard paramagnetic one
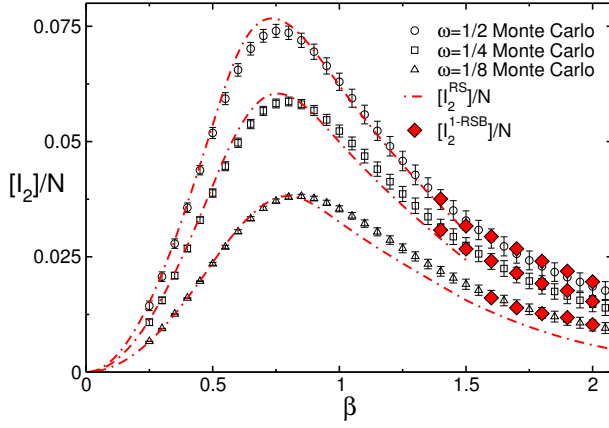
FIG. 10. The classical mutual information per spin $\mathcal{I}_2/N$ in the SK model on the 2-sheets booklet with zero magnetic field: $\mathcal{I}_2$ plotted versus β. The symbols denote the Monte Carlo results extrapolated to the thermodynamic limit for booklet ratios $\omega = 1/2, 1/4, 1/8$ (circles, squares, triangles). The dash-dotted lines are the analytical results in the replica-symmetric (RS) appproximation. The full symbols (rhombi) are the results in the first-step replica-symmetry-breaking (1-RSB) approximation.

at high temperature. The two phases are divided by a phase transition, as in the S-K model on the plane. Interestingly, the critical temperature exhibits a non-trivial dependence on ω that we determined analytically. We fully characterized the high-temperature phase of the model using the replica-symmetric (RS) approximation. Specifically, we provided the exact analytical expression for the disorder-averaged free energy $[F_{para}(\omega, n, \beta)]$ (cf. Eq. (32)) in the thermodynamic limit. On the other hand, we observed that in the glassy phase the replica symmetry has to be broken, similar to the standard S-K model. To take into account the effects of the replica symmetry breaking we used a generalization of the the Parisi ansatz[8], i.e., breaking the replica symmetry in successive steps. We restricted ourselves to the one-step replica symmetry breaking (1-RSB), providing the exact expression for the disorder-averaged free energy $F_{1\text{-}RSB}(\omega, n, \beta)$ (cf. Eq. (46)).

Finally, we compared our analytical results with Monte Carlo simulations, focusing on the internal energy per spin $U(\omega, n, \beta)/N$. In the high-temperature region, where the replica symmetry is not broken, we observed perfect agreement with the replica-symmetric result U_{RS}/N, for any ω. In the glassy phase at low temperature, we found significant deviations from U_{RS} already at $\beta \approx 1$. On the other hand, the one-step replica-symmetry-broken approximation $U_{1\text{-}RSB}/N$ matched the Monte Carlo data for $\beta \lesssim 3$.

Finally, we discussed the behavior of $[S_2]$ and $[\mathcal{I}_2]$. Due to the mean-field nature of the S-K model we observed the volume laws $[S_2] \propto N$ and $[\mathcal{I}_2] \propto N$, for any β. We considered the densities $[S_2]/N$ and $[\mathcal{I}_2]/N$. Using the replica-symmetric (RS) and the one-step replica symmetry breaking (1-RSB) approximations we provided analytical results for both $[S_2]/N$ and $[\mathcal{I}_2]/N$. We observed that at high temperature the RS result fully agrees with the Monte Carlo simula-

tions, whereas deviatios occur in the glassy phase, signalling the replica symmetry breaking. Similar to the internal energy, we found that the 1-RSB approximation fully matches the Monte Carlo data for $\beta \approx 3$. Interestingly, we numerically observed that at the critical point $\mathcal{I}_2/N$ does not show any crossing for different system sizes, in contrast with local models[28].

Our work opens several research directions. First, it would be interesting to extend our results taking into account the full breaking of the replica symmetry, i.e., going beyond the one-step replica symmetry breaking approximation. This would allow to reach a conclusion on the correctness of the replica symmetry breaking scheme that we used. Moreover, it would be interesting to discuss the finite size-corrections to the saddle point approximation. An interesting direction would be to investigate wheather the glassy behavior is reflected in the volume-law corrections to the classical Rényi entropies. Finally, it would be interesting to extend our results to *quantum* spin systems exhibiting glassy behavior and replica symmetry breaking[41,42].

X. ACKNOWLEDGEMENTS

Appendix A: The saddle point equations

In this section we provide the analytical expression for the saddle point equations (23)(24), which determine the overlap tensor $q_{\gamma\gamma'}^{rr'}$ (see section III B). We restrict ourselves zero magnetic field and to the 2-sheets booklet (see Fig. 1). It is straightforward to generalize the calculation to the case with non zero magnetic field and to the n-sheets booklet. Specifically, here we provide the saddle point equations obtained in both the replica-symmmetric (RS) (see section IV B), and the one-step replica symmetry breaking (1-RSB) approximation (see section V).

1. The replica-symmetric (RS) approximation

In the replica-symmetric approximation $q_{\gamma\gamma'}^{rr'}$ depends on the two parameters $q_0, q_0' \in \mathbb{R}$ (cf. Eq. (34)). The saddle point equations are easily derived from the RS approximation for the free energy $[F_{RS}(\omega, n, \beta)]$ (cf. Eq. (35)) as $\nabla_{\mathbf{q}}[F_{RS}(\omega, 2, \beta)] = 0$, where $\mathbf{q} \equiv (q_0, q_0')$, and $\nabla_{\mathbf{q}} \equiv \partial/\partial\mathbf{q}$. A straightforward calculation gives the two equations

$$\frac{1-q_0}{1-\omega} = 2 \int dz G_0(z)(1 + \exp(2\beta^2(q_0 - q_0'))\cosh(2z))^{-1},$$

$$\text{(A1)}$$

and

$$2\beta^2 \frac{1-q_0'}{1-\omega} = \int dz G_0(z) \Big\{ \frac{\omega}{1-\omega} \Delta_0(z) \log \cosh(2z)$$
$$+ \Delta_0(z) \log(1 + \exp(2\beta^2(q_0 - q_0')) \cosh(2z))$$
$$+ 2\beta^2(1 + \exp(2\beta^2(q_0 - q_0')) \cosh(2z))^{-1} \Big\}, \quad \text{(A2)}$$

where we defined $\Delta_0(z)$ as

$$\Delta_0(z) \equiv \frac{z^2}{2\beta^2 q_0'^2} - \frac{1}{2q_0'}, \quad \text{(A3)}$$

and the so-called heat kernel $G_0(z)$ as

$$G_0(z) \equiv \frac{1}{\sqrt{2\pi\beta^2 q_0'}} \exp\Big(- \frac{z^2}{2\beta^2 q_0'} \Big). \quad \text{(A4)}$$

Notice that $\int dz G_0(z)\Delta_0(z) = 0$.

2. The one-step replica symmetry breaking (1-RSB) approximation

In the one-step replica symmetry breaking approximation (see section V) $q_{\gamma\gamma'}^{rr'}$ depends on the four parameters

$q_0, q_0', q_1', m_1 \in \mathbb{R}$. The saddle point equations are given as $\nabla_{\mathbf{p}}[F_{1\text{-}RSB}] = 0$, where $\mathbf{p} \equiv (q_0, q_0', q_1', m_1)$, and $[F_{1\text{-}RSB}]$ is the disorder-averaged free energy given in Eq. (46). It is useful to define the modified heat kernel $G_1(z)$ as

$$G_1(z) \equiv \frac{1}{\sqrt{2\pi\beta^2(q_1' - q_0')}} \exp\Big(- \frac{z^2}{2\beta^2(q_1' - q_0')} \Big), \quad \text{(A5)}$$

and

$$\Delta_1(z) \equiv \frac{z^2}{\beta^2(q_1' - q_0')^2} - \frac{1}{q_1' - q_0'} \quad \text{(A6)}$$

$$\Gamma(z) \equiv \Big\{ \int dz' G_1(z') \cosh^{m_1}(2z + 2z') \Big\}^{-1}$$

$$\Gamma'(z) \equiv \Big\{ \int dz' G_1(z') \Big(1 + \cosh(2z + 2z') \Big)^{m_1} \Big\}^{-1}$$

$$\Theta(z, z') \equiv 1 + \exp(2\beta^2(q_0 - q_1')) \cosh(2z + 2z').$$

Finally, the saddle point equations for q_0, q_0', q_1', m_1 are obtained as

$$0 = (1 + q_0 - 2\omega)\exp(-2\beta^2(q_0 - q_1')) - 2(1-\omega)\int dz dz' G_0(z)\Gamma'(z)G_1(z')\cosh(2z + 2z')\Theta^{m_1-1}(z, z') \quad \text{(A7)}$$

$$0 = 4\beta^2 m_1 q_0' + \frac{\omega}{m_1}\int dz G_0(z)\Delta_0(z)\log\int dz' G_1(z')\cosh^{m_1}(2z + 2z')$$
$$+ \frac{1-\omega}{m_1}\int dz G_0(z)\Delta(z)\log\int dz' G_1(z')\Theta^{m_1}(z, z') - \frac{\omega}{m_1}\int dz dz' G_0(z)\Gamma(z)G_1(z')\Delta_1(z')\cosh^{m_1}(2z + 2z')$$
$$- \frac{1-\omega}{m_1}\int dz dz' G_0(z)\Gamma'(z)G_1(z')\Delta_1(z')\Theta^{m_1}(z, z') \quad \text{(A8)}$$

$$0 = -4\beta^2(m_1 - 1)q_1' - 4\beta^2\omega + \frac{\omega}{m_1}\int dz dz' G_0(z)\Gamma(z)G_1(z')\Delta_1(z')\cosh^{m_1}(2z + 2z')$$
$$+ \frac{1-\omega}{m_1}\int dz dz' G_0(z)\Gamma'(z)G_1(z')\Big\{ \Delta_1(z')\Theta^{m_1}(z, z') - 4\beta^2 m_1 \exp(2\beta^2(q_0 - q_1'))\cosh(2z + 2z')\Theta^{m_1-1}(z, z') \Big\} \quad \text{(A9)}$$

$$0 = -\beta^2(q_1'^2 - q_0'^2) + \frac{\omega}{m_1}\int dz dz' G_0(z)\Gamma(z)G_1(z')\cosh^{m_1}(2z + 2z')\log\cosh(2z + 2z')$$
$$+ \frac{1-\omega}{m_1}\int dz dz' G_0(z)\Gamma'(z)G_1(z')\Theta^{m_1}(z, z')\log(\Theta(z, z')) - \frac{1-\omega}{m_1^2}\int dz G_0(z)\log\int dz' G_1(z')\Theta^{m_1}(z, z')$$
$$- \frac{\omega}{m_1^2}\int dz G_0(z)\log\int dz' G_1(z')\cosh^{m_1}(2z + 2z'). \quad \text{(A10)}$$

Appendix B: Monte Carlo method to calculate the classical Rényi entropies

Here we describe the Monte Carlo method that we used to calculate the Rényi entropies S_n and the mutual information

$\mathcal{I}_n$. The method exploits the representation of S_n as ratio of

partition functions as

$$S_n(A) \equiv \frac{1}{1-n} \log \left(\frac{Z(A,n,\beta)}{Z^n(\beta)} \right), \qquad \text{(B1)}$$

where $Z(A,n,\beta)$ and $Z(\beta)$ are the partition functions of the model on the booklet and on the plane, respectively (see Fig. 1 and section II for the definitions). There are a only few approaches to numerically calculate the the ratio of partition functions in Eq. (B1). For instance, a brute force numerical integration of the internal energy as a function of temperature[28] can be used to calculate $Z(A,n,\beta)$ and $Z(\beta)$. However, this requires high accuracy over a large range of temperature.

Here we directly calculate the ratio of partition functions in Eq. (B1) using the so-called *ratio trick*. In the ratio trick one splits the subsystem A as $A = \sum_i A_i$, where A_i is a sequence of subsystems such that $A_i \subset A_{i+1}$. Then one writes

$$\frac{Z(A,n,\beta)}{Z^n(\beta)} = \prod_{i=0}^{N/4-1} \frac{Z(A_i,n,\beta)}{Z(A_{i+1},n,\beta)} \qquad \text{(B2)}$$

where for simplicity we specialized to intervals A_i such that

$$A_i = 4i, \quad i \in [0, N/4]. \qquad \text{(B3)}$$

Crucially, if the length of A_i increases mildly with i, each term in the product in the left hand side of (B2) can be sampled efficiently in Monte Carlo[29]. Notice that a similar method has also been used in Ref. 43–45. More specifically, one can write

$$\frac{Z(A_i,n,\beta)}{Z(A_j,n,\beta)} = \frac{T_{j \to i}}{T_{i \to j}} \qquad \text{(B4)}$$

where $T_{i \to j}$ is the (Monte Carlo) transition probability from a spin configuration living on the booklet with $A = A_i$ to a spin configuration living on the booklet with $A = A_j$. Notice that spins in region A of different sheets are identified (cf. Eq. (9)). Clearly, if $j < i$ one has $T_{i \to j} = 1$. When $j > i$ a naive method to determine $T_{i \to j}$ would be to simply count the fraction of times (during the Monte Carlo update) that a spin configuration living on the booklet with $A = A_i$ is also a valid spin configuration on the booklet with $A = A_j$. In the following we provide a more efficient scheme to calculate $T_{i \to j}$.

To summarize, our approach for calculating the ratio of partition functions in Eq. (B2) consists of four steps:

1. Do a full Monte Carlo sweep of the system on the booklet with $A = A_i$ to generate an importance sampled spin configuration. This can be done with any update scheme, such as standard Metropolis or cluster updates

2. For the the spins living in $A_{i+1} - A_i$ calculate

$$W_a = \sum_i e^{-\beta E_i}. \qquad \text{(B5)}$$

Here (cf. Eq. (B3)) i runs over all the $n2^4$ configurations of the four spins in $A_{i+1} - A_i$, and E_i is the energy associated with configuration i.

3. Calculate the quantity

$$W_b = \sum_j e^{-\beta E_j} \qquad \text{(B6)}$$

where j runs over all the 2^4 configurations with the four spins living in $A_{i+1} - A_i$ and different sheets are identified.

4. Calculate the transition probability $T_{i \to i+1}$ as

$$T_{i \to i+1} = \left\langle \frac{W_b}{W_a} \right\rangle. \qquad \text{(B7)}$$

This method is much faster than simply counting configurations as it allows us to integrate over all possible configurations of the spins in $A_{i+1} - A_i$, treating the remaining ones as a bath that is updated by the regular Monte Carlo update. The computational cost of this procedure grows exponentially with the number of spins in $A_{i+1} - A_i$.

In our Monte Carlo simulations we calculate $Z(A_i,n,\beta)/Z(A_{i+1},n,\beta)$ for every disorder realization and $S_n(A)$ using Eq. (B1). Finally, we average over the disorder to obtain $[S_n(A)]$.

1 K. Binder and A. P. Young, Rev. Mod. Phys. **58**, 801 (1986).
2 M. Mezard, G. Parisi, and M. Virasoro, *Spin Glass theory and beyond*, World Scientific, Singapore (1987).
3 A. P. Young, *Spin Glasses and Random Fields* (Singapore: World Scientific).
4 H. Nishimori, "Statistical Physics of Spin Glasses and Information Processing", Clarendon Press, Oxford (2001).
5 T. Castellani and A. Cavagna, J. Stat. Mech. (2005) P05012.
6 D. Sherrington and S. Kirkpatrick, Phys. Rev. B **17**, 4385 (1978).
7 D. Sherrington and S. Kirkpatrick, Phys. Rev. Lett. **35**, 1972 (1978).
8 G. Parisi, J. Phys. A **13**, 1101 (1980).
9 M. Talagrand, Ann. of Math. **163**, 221 (2006).
10 L. A. Pastur and M. V. Shcherbina, J. Stat. Phys. **62**, 1 (1991).

11 M. Mezard, G. Parisi, N. Sourlas, G. Toulouse, and M. Virasoro, Phys. Rev. Lett. **52**, 1156 (1984).
12 R. Rammal, G. Toulouse, and M. A. Virasoro, Rev. Mod. Phys. **58**, 765 (1986).
13 J. Cardy, *Scaling and Renormalization in Statistical Physics* (Cambridge Lecture Notes in Physics).
14 B. Yucesoy, H. G. Katzgraber, and J. Machta, Phys. Rev. Lett. **109**, 177204 (2012).
15 A. Billoire, L. A. Fernandez, A. Maiorano, E. Marinari, V. Martin-Mayor, G. Parisi, F. Ricci-Tersenghi, J. J. Ruiz-Lorenzo, and D. Yllanes, Phys. Rev. Lett. **110**, 219701 (2013).
16 B. Yucesoy, H. G. Katzgraber, and J. Machta, Phys. Rev. Lett. **110**, 219702 (2013)
17 S. Morrison, A. Kantian, A. J. Daley, H. G. Katzgraber,

M. Lewenstein, H. P. Büchler, and P. Zoller, New J. Phys. **10**, 073032 (2008).

[18] P. Rotondo, E. Tesio, and S. Caracciolo, Phys. Rev. B **91**, 014415 (2015).

[19] N. Ghofraniha, I. Viola, F. Di Maria, G. Barbarella, G. Gigli, L. Leuzzi, and C. Conti, Nature Comm. **6**, 6058 (2015).

[20] L. Amico, R. Fazio, A. Osterloh, and V. Vedral, Entanglement in Many-Body Systems, Rev. Mod. Phys. **80**, 517 (2008).

[21] J. Eisert, M. Cramer, and M. B. Plenio, Area laws for the entanglement entropy - a review, Rev. Mod. Phys. **82**, 277 (2009).

[22] P. Calabrese, J. Cardy, and B. Doyon Eds., Special issue: Entanglement entropy in extended systems, J. Phys. A **42**, 50 (2009).

[23] P. Calabrese and J. Cardy, Entanglement entropy and conformal field theory, J. Phys. A **42** 504005 (2009).

[24] C. Holzhey, F. Larsen, and F. Wilczek, Geometric and Renormalized Entropy in Conformal Field Theory, Nucl. Phys. B **424**, 443 (1994).

[25] G. Vidal, J. I. Latorre, E. Rico, and A. Kitaev, Entanglement in quantum critical phenomena, Phys. Rev. Lett. **90**, 227902 (2003). J. I. Latorre, E. Rico, and G. Vidal, Ground state entanglement in quantum spin chains, Quant. Inf. and Comp. **4**, 048 (2004).

[26] P. Calabrese and J. Cardy, Entanglement entropy and quantum field theory, J. Stat. Mech. (2004) P06002. P. Calabrese and J. Cardy, Entanglement entropy and quantum field theory: a non-technical introduction, Int. J. Quant. Inf. **4**, 429 (2006).

[27] P. Calabrese, J. Cardy, and E. Tonni, Phys. Rev. Lett. **109**, 130502 (2012).

[28] J. Iaconis, S. Inglis, A. B. Kallin, and R. G. Melko, Phys. Rev. B **87**, 195134 (2013).

[29] J.-M. Stéphan, S. Inglis, P. Fendley, and R. G. Melko, Phys. Rev. Lett. **112**, 127204 (2014).

[30] F. C. Alcaraz and M. A. Rajabpour, Phys. Rev. Lett. **111**, 017201 (2013).

[31] J.-M. Stéphan, Phys. Rev. B **90**, 045424 (2014).

[32] M. M. Wolf, F. Verstraete, M. B. Hastings, and J. I. Cirac, Phys. Rev. Lett. **100**, 070502 (2008).

[33] G. Refael and J. E. Moore J. Phys. A: Math. Theor. **42** 504010 (2009).

[34] C. Castelnovo, C. Chamon, and D. Sherrington, Phys. Rev. B **81**, 184303 (2010).

[35] G. Parisi, Phys. Rev. Lett. **43**, 1754 (1979).

[36] F. Guerra and F. L. Toninelli, Commun. Math. Phys. **230**, 71 (2002).

[37] J. R. L. de Almeida and D. J. Thouless, J. Phys. A **11**, 983 (1978).

[38] A. Billoire, in *Rugged Free Energy Landscape*, Springer Lecture Notes in Physics, edited by W. Janke (Springer, Berlin-Heidelberg 2007.

[39] T. Aspelmeier, A. Billoire, E. Marinari, and M. A. Moore, J. Phys. A: Math. Theor. **41** 324008 (2008).

[40] G. Parisi, Phys. Rev. Lett **50**, 1946 (1983).

[41] N. Read, S. Sachdev, and J. Ye, Phys. Rev. B **52**, 384 (1995).

[42] A. Andreanov and M. Müller, Phys. Rev. Lett. **109**, 177201 (2012).

[43] V. Alba, L. Tagliacozzo, and P. Calabrese, Phys. Rev. B **81**, 060411(R) (2010).

[44] V. Alba, L. Tagliacozzo, and P. Calabrese, J. Stat. Mech. (2011) P06012.

[45] V. Alba, J. Stat. Mech. (2013) P05013.